

## **A local view of the laser induced magnetic domain dynamics in CoPd stripe domains at the picosecond time scale.**

V. López-Flores<sup>1</sup>, M.-A. Mawass<sup>1,2</sup>, J. Herrero-Albillos<sup>2</sup>, A. Uenal<sup>2</sup>, S. Valencia<sup>2</sup>, F. Kronast<sup>2</sup>, and C. Boeglin<sup>1\*</sup>

<sup>1</sup> Université de Strasbourg, CNRS, Institut de Physique et Chimie des Matériaux de Strasbourg, UMR 7504, F-67000 Strasbourg, France.

<sup>2</sup> Institut für Methoden und Instrumentierung der Forschung mit Synchrotronstrahlung Helmholtz-Zentrum Berlin für Materialien und Energie GmbH, Albert-Einstein-Str. 15, 12489 Berlin, Germany

\* *Corresponding author:*

*Mel:* [christine.boeglin@ipcms.unistra.fr](mailto:christine.boeglin@ipcms.unistra.fr)

*Address:* Institut de Physique et de Chimie des Matériaux de Strasbourg (IPCMS)

23, rue du Loess 67034 Strasbourg

### **Abstract**

The dynamic of the magnetic structure in a well ordered ferromagnetic CoPd stripe domain pattern has been investigated upon excitation by femtosecond infrared laser pulses. Time-resolved X-ray magnetic circular dichroism in photoemission electron microscopy (TR-XMCD-PEEM) is used to perform real space magnetic imaging with 100 ps time resolution in order to show local transformations of the domains structures. Using the time resolution of the synchrotron HZB-BESSY II, we are able to image the transient magnetic domains in a repetitive pump and probe experiment. In this work, we study the reversible and irreversible transformations of the excited magnetic stripe domains as a function of the laser fluence. Our results can be explained by thermal contributions, reducing the XMCD amplitude in each stripe domain below a threshold fluence of 12 mJ/cm<sup>2</sup>. Above this threshold fluence, irreversible transformations of the magnetic domains are observed. Static XMCD-PEEM images reveal the new partially ordered stripe domain structures characterized by a new local magnetic domain pattern showing organized pattern at the micrometer scale. The new arrangement is attributed to the recovery of the magnetic anisotropy during heat dissipation under an Oersted field.

## 1. Introduction

Femtosecond laser excitation on ferromagnetic films leads to a macroscopic ultrafast demagnetization on a sub-picosecond time scale [1]. This pioneering work opened the field of femtomagnetism extending nowadays to several aspects. [1, 2, 3, 4, 5, 6, 7, 8]. One of the most challenging aspects studied in recent years in this field is the dynamic response of magnetic domains to such excitations. One of those having attracted a lot of attention is the laser induced switching of the magnetization [5, 9]. During the past years the study of the dynamics of the spins in magnetic domains have motivated many studies addressing different aspects of the dynamical processes, discussing Elliot Yafet or thermal effects as well as Circular dichroism effects as possible mechanisms to understand the switching of spins. However, complex magnetic domain transformations triggered by laser excitations have been studied by several groups [5, 9, 10 - 13] and show that the ultrafast switching dynamics are far from being understood. Most of these experiments have been performed by magneto-optic Kerr effect. Although time resolutions down to 50 fs can be achieved by means of ultrafast Kerr microscopy, this technique shows a limited lateral resolution [14]. This drawback can be overcome by using synchrotron-based techniques within the soft X-ray energy range combining magnetic and element-resolution with  $\sim 10$  nm spatial resolution. Recent advances on time-resolved X-ray techniques (synchrotrons, X-FEL and HHG laser sources) have improved the understanding of the spin dynamics in single and multidomain structures [3, 6, 10, 11]. Techniques based on X-ray magnetic circular dichroism (XMCD) could recently provide new information's in order to describe the dynamics of spins upon laser excitations. [3, 6, 13]. However, combining the ultimate time and space resolution in order to describe ultrafast domain dynamics, is still a challenge. Several X-ray based techniques have been used revealing different aspects of the dynamics of the micromagnetic domains with various time resolutions [10 - 13, 15 - 20]. Although sub-picosecond time resolution using resonant X-ray scattering only provide average information and many local aspects of the domain organisation are missing. Moreover, using X-ray holography techniques [19], the field of view is usually too small to capture specific and local dynamics in the domains. A recent study using time-resolved resonant magnetic X-ray scattering showed that IR pump pulses induce demagnetization and reorientation of the magnetic domains in CoPd stripe patterns [12]. This study could provide average parameters at the nanosecond timescale describing the recovery of the magnetic pattern after a single intense IR pump.

We show here that a real space view of the picosecond demagnetization dynamics in CoPd stripe domains can reveal new aspects of the local transformations of domains upon femtosecond laser excitations. Such study can be performed using X-ray photoemission electron microscopy (XPEEM) operated in a pump-probe configuration with few tens of picosecond time resolution. It combines adequate spatial resolution of 30 nm in order to describe the local picosecond dynamics of the magnetic domains after laser excitation [16, 17]. Both the reversible and the irreversible transformations induced by the IR laser have been addressed in our study. The two different regimes of transformations of the domain structures are obtained below and above a threshold pump fluence of  $12 \text{ mJ/cm}^2$  corresponding to the reversible pump conditions used for CoPd films in our previous studies [6, 7, 10, 12, 19].

Our results show that exploiting the quantitative XMCD-PEEM images, the laser induced quenching of ferromagnetic stripe domains proceeds by a reduction of the magnetization inside the magnetic domains and probably broadening of the domain walls. We show that this transformation also involves a thermal induced partial transfer of the magnetization from out-of-plane to in-plane. The laser induced evolution of the magnetic stripe pattern is reproduced by micromagnetic simulations based on the temperature dependent anisotropy in CoPd.

## 2. Experiment

### 2.1 Samples

The 50 nm thick magnetic films are deposited at 423 K on top of a conductive doped Si substrate by means of electron beam co-evaporation of Co and Pd from highly pure target metals. The thickness of the layer and the alloy composition of  $\text{Co}_{0.60}\text{Pd}_{0.40}$ , ensured regular magnetic stripe domains and a large out of plane anisotropy in the film. The parallel stripes, showing typical lateral sizes of 80 nm, were induced in the samples by an in-plane demagnetization procedure. The maximum applied field was 1.6 T, and the reduction rate was 1% of the previous step, until 5 mT, where the field was reduced to 0. Due to the magnetic anisotropy, alternated out-of-plane stripe domains are formed with the stripes orienting parallel to the demagnetizing field [21]. Following this procedure many static and dynamic Magnetic Force Microscopy (MFM) or XMCD-based experiments have been conducted in the past [10, 12, 13, 20, 21- 24].

The base pressure during co-evaporation was  $1 \times 10^{-9}$  mbar. A 20 nm Pd buffer layer was deposited to provide an efficient transfer of the pump induced heat. A 2 nm Pd + 1 nm Al capping layer was used to prevent oxidation of the magnetic layer. No oxidation could be evidenced at the  $\text{CoL}_3$  edge during our experiment.

SQUID measurements were carried out to characterize the out-of-plane anisotropy of the samples. Both in-plane and out-of-plane magnetizations were measured as a function of the temperature to determine the temperature dependence of the magnetic anisotropy. As shown in Figure 1, the in-plane component of the saturation magnetization is large and becomes stronger the higher the temperature, while the out-of-plane component becomes weaker. This temperature dependence is compatible with the temperature dependent anisotropy constant of the CoPd film.

### 2.2 Experimental Configuration

X-ray photoemission electron microscopy (X-PEEM) measurements were carried out at the UE49/2-PGM-SPEEM beamline at BESSY II synchrotron (Helmholtz Zentrum Berlin). The experimental setup is described elsewhere [27]. The magnetic contrast on the X-PEEM is achieved by taking advantage of sensitivity to ferromagnetic domain direction of the X-ray magnetic circular dichroism (XMCD) effect at the  $L_{2,3}$  edges of transition metals. Accordingly, we collected X-PEEM images at the  $\text{Co-L}_3$  edge (778 eV) with both left- and right-handed circularly polarized light. Their subtraction divided by their sum leads to the XMCD *asymmetry image*, which contrast arises from magnetic domains only, and which intensity and sign depends on the projection of the magnetization along the incident X-ray direction.

The pump laser is a Ti:Sapphire laser system operating at 800 nm wavelength and 100 fs pulse width with a repetition rate of 5 MHz. The laser and the X rays impinge on the surface of the film with an incidence angle of  $16^\circ$  from the surface plane. By operating the microscope at a field of view of 5  $\mu\text{m}$ , we ensure to image the surface of the CoPd film homogeneously excited by the IR laser. This is due to the fact that the laser spot on the sample is  $60 \times 20 \mu\text{m}^2$  which is larger than the trace of the X-ray spot ( $30 \times 10 \mu\text{m}^2$ ). Moreover, the penetration depth of the IR laser for the CoPd alloy (10 nm) is smaller than the XMCD-PEEM probing depth (2-5 nm), guarantees that the probed region is homogeneously excited in depth as well.

For the time-resolved pump-probe experiments we used the single-bunch filling mode of BESSY synchrotron, which produces a single X-ray pulse with a frequency of 1.25 MHz and width about 60 ps. The experiment leads to an XMCD-PEEM imaging with an estimated time resolution of 60 ps.

Additionally, the multi-bunch X-ray beam was used to characterize the static stripe pattern configuration before any laser excitation and after the series of pump-probe experiments.

During the time-resolved experiment, the laser pump pulse was synchronized with the X-ray probe pulse by a phase locked loop (PLL) circuit. The time overlap between X rays and IR laser pulse was detected exploiting the burst of secondary electrons at a defect resonating with the laser. An electromechanical trombone delay line was used to shift the phase of the storage ring master clock signal used for synchronization, defining the phase shift of the IR-laser and thereby the pump-probe delay.

Time-resolved XMCD-PEEM images were taken at room temperature at two different pump-probe delays: -250 ps and +190 ps. At these two delays, time resolved and time integrated XMCD-PEEM images were taken at different IR laser fluences. The sequences of images characterises the laser induced demagnetization and re-organisation of the magnetic stripe pattern.

Irreversible transformations of the stripe pattern have been observed by recording time integrated XMCD-PEEM images at different laser fluences between 8-18 mJ/cm<sup>2</sup> until the irreversible damage threshold was reached (above 12 mJ/cm<sup>2</sup>). We repeat this study for different in-plane directions of the magnetic stripe domains (35° and 90 °) in respect to the X-ray propagation direction.

### 3. Experimental results

#### *Dynamics of magnetic stripe domains.*

The XMCD-PEEM characterization previous to any laser exposure confirms the presence of magnetic stripes at room temperature shown in figure 2(a). The blue and red contrast results from the projection of the out-of-plane magnetization to the X-ray propagation direction. As shown by the Fourier Transformation (F.T.) of the PEEM image of magnetic domains (see inset in Fig. 2a) the presence of two spots evidences the periodicity of the ordered magnetic stripes perpendicular to the X-ray incidence.

Time-resolved XMCD-PEEM images recorded at -250 ps before (left) and at +190 ps after the laser excitation is shown in Figures 2b-g for different laser fluences  $F$  ( $F= 8.8; 9.5$  and  $10.7$  mJ/cm<sup>2</sup>).

Due to the repetitive pump-probe, an IR fluence dependent DC heating increases the mean XMCD values at any delays. This corresponds to the increase of the in-plane component of the magnetization as measured by the grazing incident X rays and is confirmed by the temperature dependent SQUID data. In order to visualize the typical effects of the DC heating on our time-resolved XMCD-PEEM images, we plot in the insert of Figure 2 (top right) 3 qualitative line profiles representing the local XMCD values and the temperature induced offsets across the stripe domains. The colour code (blue-white-red) qualitatively reproduces the colour codes observed in our XMCD-PEEM images and is proportional to the normalized XMCD. The drawn continuous lines (black, green, and yellow) evidence the local magnetization across 3 successive stripe domains and domain walls. Our sketch qualitatively describes typical line profiles perpendicular to the stripe direction and shows 3 different stripe domain configurations: Without laser (black line), with laser at a delay of -250 ps (green line) and with laser at a delay of +190 ps (yellow line). A XMCD offset shift towards higher XMCD values is shown by green and yellow dashed lines for both delays -250 ps and +190ps. The offset value is given by the average XMCD through the domain pattern and is proportional to the DC heating.

The yellow curve reproducing the magnetization across the domain wall at positive delay of +190 ps reproduces the well known enlarged domain wall. This line profile follows qualitatively the OOMMFS simulations which are shown in Figure 3.

The simulated magnetic line profiles have been obtained for a 50 nm thick CoPd alloy film for two different and realistic values of the magnetic anisotropy constants defining the system at room temperature and at an elevated temperature,  $K_m=5e6 \text{ J/m}^3$  and  $K_m=5e5 \text{ J/m}^3$ , respectively. The magnetic parameters for the CoPd alloy have been taken from literature [12, 22, 25, 26]. The OOMMF simulated line profiles evidence the change of the domain wall between two up and down domains. Comparing the two simulated profiles we identify the effect of temperature on the domain walls. As expected, we obtain wider domain walls at an elevated temperature. One notices that at lower anisotropy the domain wall thickness is broader (from  $\sim 3\text{nm}$  to  $\sim 15 \text{ nm}$  when the anisotropy is divided by 10). Unfortunately, this modification cannot be imaged with XMCD-PEEM, because it is below our experimental spatial resolution of 30 nm.

Furthermore, at a given pump fluence, the XMCD offset (Figure 2 (top right)) is slightly stronger for the delays at +190 ps than for -250 ps (yellow compared to green dashed lines). This is present at any IR fluences and corresponds to the time-dependent increase of the in-plane component of the magnetization (as suggested by the temperature dependent SQUID data). Table 1 shows the mean XMCD extracted values from the PEEM images, taking into account the geometry of the experiment. The extracted value of the reference image Figure 2a without laser is close to 0% corresponding to an equal number of up and down magnetic domains. One notices that at a delay of -250 ps the DC heating induces a mean XMCD value of 10% which noticeably decreases for higher IR pump fluences ( $F= 9.5$  and  $10.7 \text{ mJ/cm}^2$ ). At moderate IR fluence of  $F=8.8 \text{ mJ/cm}^2$  we interpret the large XMCD mean value as related to a sizable heat induced in-plane component combined with a lower out of plane magnetization contrast (green line in sketch). At larger IR fluences of  $F = 9.5$  and  $10.7 \text{ mJ/cm}^2$  the mean XMCD decreases by -50 % and -65 % respectively. Such a significant drop can only be interpreted by temperature induced demagnetization along both, the in-plane and out-of-plane direction.

At a delay of +190 ps we extract from Table 1 the mean XMCD values which are consistently higher for all images compared with their counterpart at -250 ps. The +2% increase of the overage XMCD values at  $t = +190 \text{ ps}$  reflects a time-dependent thermal induced magnetization rotation from out of plane to in-plane, driven by a lower magnetic anisotropy at +190 ps. This is indeed verified by comparing the local XMCD amplitudes of the magnetic stripe domains at -250 ps and +190ps as sketched in Figure 2 (top right - yellow line).

To quantify the reduction of the XMCD amplitude (prop. to magnetisation in the up and down magnetic domains) we performed a 2D Fourier transformation (FT) of the XMCD-PEEM images. They are shown in figure 2 as insets. Using the FT we are able to focus and analyze the changes in the spatial distribution of the observed intensities. The azimuthal intensity distribution  $I(\Phi)$  yields a characterization of the ordering and the correlation length of the magnetic domains. However, because of the poor FT data quality, related to the limited  $5 \mu\text{m}$  spatial integration, we will limit our analysis to the normalized azimuthal scattering intensity distributions as shown in figure 4 (using a 2 degree step). We normalize the azimuthal intensity distribution  $I(\Phi)$  by the background level of the FT image. In this way we can exploit the peak intensities and their half maximum to characterise the average magnetization in the domains and their correlation length.

From figure 4, it appears that the XMCD amplitudes are slightly reduced for all FT -XMCD-PEEM images at +190 ps, corresponding to the transient laser induced reduction of the magnetization in the domains (Figure 4 at fluence  $F = 8.8, 9.5$  and  $10.7 \text{ mJ/cm}^2$ ). At these delays, we evidence the transient demagnetization of -30% and -50 % in the up and down oriented magnetic strip domains, which are mainly due to thermal excitations. Indeed at delays of  $\sim 100 - 500 \text{ ps}$ , it is well known that the system has not yet reached the recovery [6, 12].

At the delay of -250 ps, (continuous lines) the reduction of the peak intensities with increasing fluences illustrates the effect due to DC heating on the magnetization of the stripe domains. However no discrimination between in-plane and out-of-plane spin directions is possible.

Furthermore, we observe in Figure 4 a change in the full width at half maximum (FWHM) from  $58^\circ$  without laser (black line), down to  $40^\circ$  for the other cases. The reduced FWHM evidences a larger correlation length of the magnetic domains. In the XMCD –PEEM images one could also notice less labyrinth-like domains after exposure to the laser (Fig 2 b, c, d, f). No significant differences are observed between -250 ps and +190ps, confirming that this effect is linked to the DC heat induced reorganisation of the stripe pattern.

#### *Domain reorientation.*

In order to describe the irreversible transformations of the stripe domains at higher laser fluences we have studied the change of static XMCD –PEEM images without and with the pump laser on the surface of the CoPd film. The static imaging mode with 15-18 mJ/cm<sup>2</sup> has been used ensuring that the previously defined threshold fluence of 12 mJ/cm<sup>2</sup> was overcome. In order to describe in-plane components of the spin as well as the stripe domains themselves we recorded and compare two different sample azimuths in respect of the incoming X rays. In the first one we orient the stripes perpendicularly to the X-ray incidence (Fig. 5a) and in the second, we orient the stripes nearly parallel ( $\sim 30^\circ$ ) to the X rays (Fig. 5c). In this last sample orientation, both the out-of-plane and in-plane spin components (projections) are visible whereas in Fig 5a only the up and down spins are visible. We therefore conclude that the magnetization of the sample is not purely out-of-plane, but is slightly tilted along the stripe direction at room temperature. We again performed the FT of the images in order to highlight the stripe orientations. In the FT image of Fig. 5c (inset) we observe that due to the contributions of the in-plane projections, an additional structure with a non-symmetrical spiral shape appears. This structure is absent in the FT image in Fig. 5a (inset).

After having submitted the CoPd film surface to the laser, we performed XMCD-PEEM imaging at room temperature for both orientations. The results are shown in Fig 5b and 5d. We note that the two magnetic domain images recorded without pump laser, at room temperature are obtained at different sample positions.

In Figure 5b we evidence that nearly half of the field of view on the right side of the image shows an almost uniform contrast corresponding to a magnetic domain that have irreversibly turned the magnetization to the in-plane direction with a strong component parallel to the X rays (red background). Over the complete field of view one can notice a new stripe ordering, confirmed by the FT shown in the inset of Figure 5b. The new alignment of the stripe domains is no more perpendicular to the X-rays incident direction and allows now to observe the in-plane components of the spins together with the stripe structures. Such a re-orientation process has already been shown and explained in our recent work [12]. However we have here access to the local view of the new domain organisation as well as in-plane projection of the spins. We can also confirm the re-orientation along a given angle of  $60^\circ$  in respect to the X-ray incidence induced by large pump fluences. By performing the same experiment with the second orientation of the stripes at  $35^\circ$  to the X rays we are able to reproduce this final state of the domain structure and reorientation (Fig 5d). We conclude that the final domain structure is independent from the initial orientation of the stripe domains. The reorientation can be confirmed in the FT diagram depicted in the corresponding insets where besides a  $60^\circ$  new alignment from the X-ray incidence we also observe a weakening of their intensities. In more details the orientation of the stripes can be analysed using the azimuthal intensity distribution  $I(\Phi)$  in figure 6. In fig 6a (black line), we follow the azimuthal distribution  $I(\Phi)$  for the initial orientation of the stripes perpendicular to the X rays (corresponding to Fig 5a). In Fig. 6b (black line) we plot  $I(\Phi)$  for the second initial orientation of the stripes, at  $35^\circ$  to the X rays. We notice that the intensity of the spots for the original perpendicular orientation is more intense than the others due to the negligible contribution of the in-plane components. Moreover, the laser induced reorientation shows reduced  $I(\Phi)$  intensities and a common final reorientation angle of  $60^\circ$

from the X rays (Fig. 6 a, b).

Comparing both cases, we can conclude that the reorientation does depend neither on the sample original geometry nor on the incidence plane of the laser or X-ray. Thus, we believe that an external cause, likely an external magnetic field, might be causing this preferential reorientation. Such a mechanism could be confirmed by micromagnetic simulations in our previous work [12].

#### **4. Conclusions**

The dynamic of the magnetic stripe domain structure have been investigated upon excitation by femtosecond infrared laser pulses. Time-resolved XMCD-PEEM reveals the transient magnetic domains as well as final domain structures at room temperature. we studied the reversible and irreversible transformations of the excited magnetic stripe domains as a function of the laser fluence. We show that at moderate laser fluences below  $12 \text{ mJ/cm}^2$ , thermal contributions reducing the XMCD amplitudes in each stripe domains are present, in parallel with increasing in-plane components of the magnetization. At larger fluences, XMCD-PEEM images reveal the new partially ordered stripe domain structures characterized by a new local magnetic domain pattern showing organized pattern at the micrometer scale. We provide a local real space description of these new magnetic domains and show that they are independent from the initial stripe configurations.

We confirm the mechanism inducing such reorganisation of stripe domains in CoPd films, considering the recovery of the magnetic anisotropy during the heat dissipation under an external Oersted field.

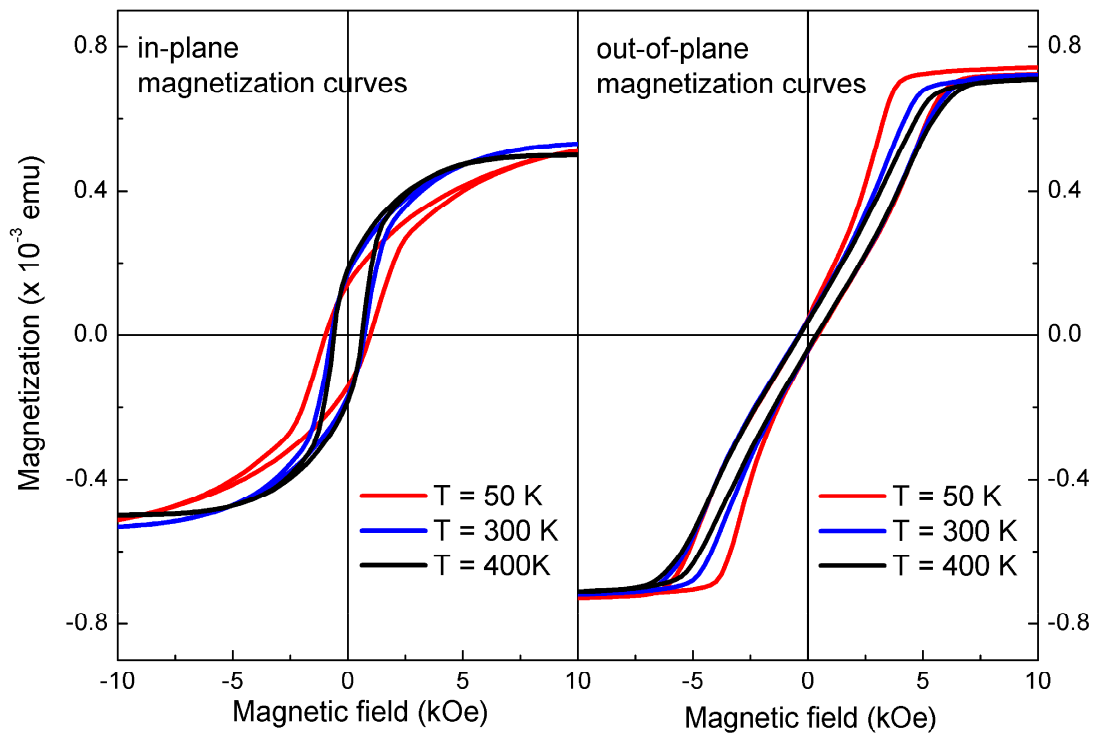


**Figure 1:** SQUID magnetometry measurements showing the magnetization of the sample at different temperatures along the in-plane (left), and out-of-plane direction (right).



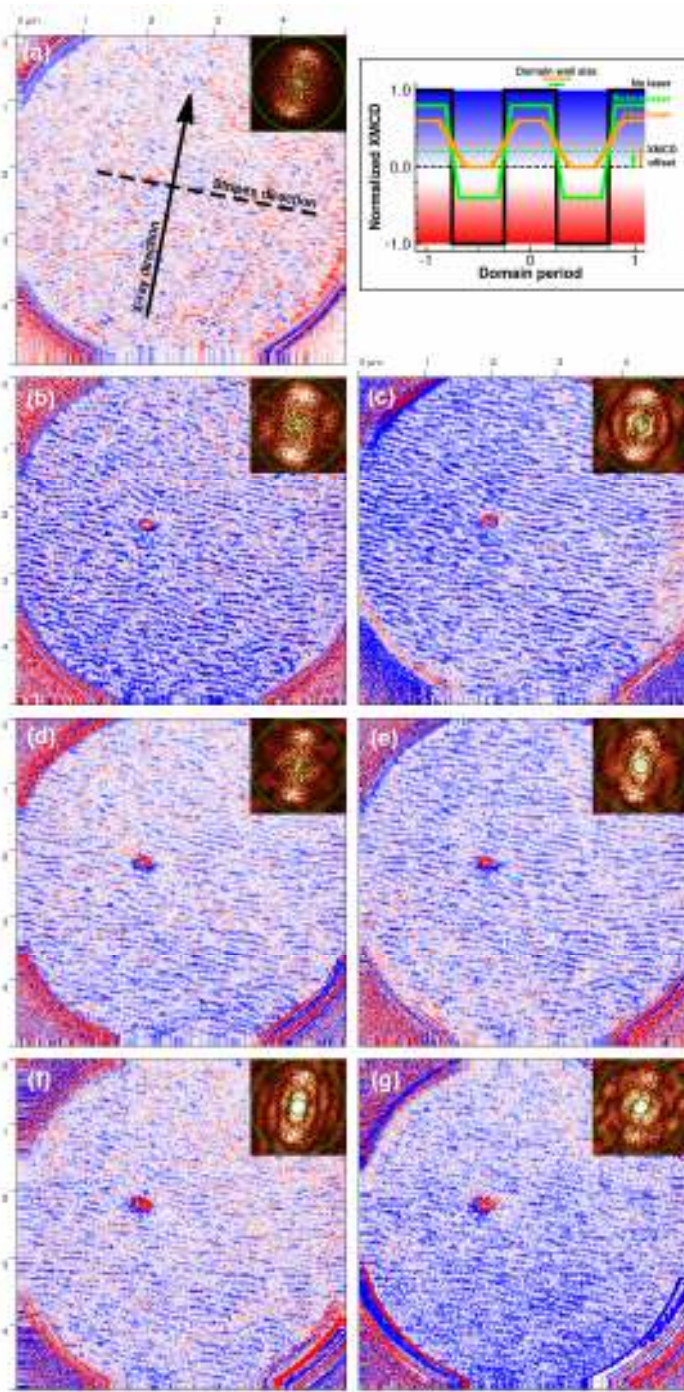


**Figure 2:** Time-resolved XMCD-PEEM images of the sample with stripes oriented  $90^\circ$  from the X-ray incidence. (a) XMCD-PEEM image without any laser applied at room temperature; (b) Time resolved XMCD-PEEM image recorded with an IR fluence of  $8.8 \text{ mJ/cm}^2$  at  $t = -250 \text{ ps}$ ; (c) Time resolved XMCD-PEEM image recorded with an IR fluence of  $8.8 \text{ mJ/cm}^2$  at  $t = +190 \text{ ps}$ ; (d) with fluence of  $9.5 \text{ mJ/cm}^2$  at  $t = -250 \text{ ps}$ ; (e) with fluence of  $9.5 \text{ mJ/cm}^2$  at  $t = +190 \text{ ps}$ ; (f) with fluence of  $10.7 \text{ mJ/cm}^2$  at  $t = -250 \text{ ps}$ ; (g) with fluence of  $10.7 \text{ mJ/cm}^2$  at  $t = +190 \text{ ps}$ ; The insets show the corresponding Fourier Transform of the images.

The top-left inset sketches a qualitative representation of the profile line intensities for 3 different XMCD-PEEM configurations (ex: figure a, b, and c).

It shows 3 line scans perpendicular to the stripe direction, as observed in our XMCD-PEEM images for 3 different stripe domain configurations: Without laser (black line), with laser at a delay of  $-250$

ps (green line) and with laser at a delay of +190 ps (yellow line). The drawn continuous lines (black, green, and yellow) evidence the local magnetization across the domain walls. An XMCD offset shift towards higher XMCD values is shown by green and yellow dashed lines for both delays -250 ps and +190ps. The blue-white-red color scale is related to the color code at the X-PEEM images

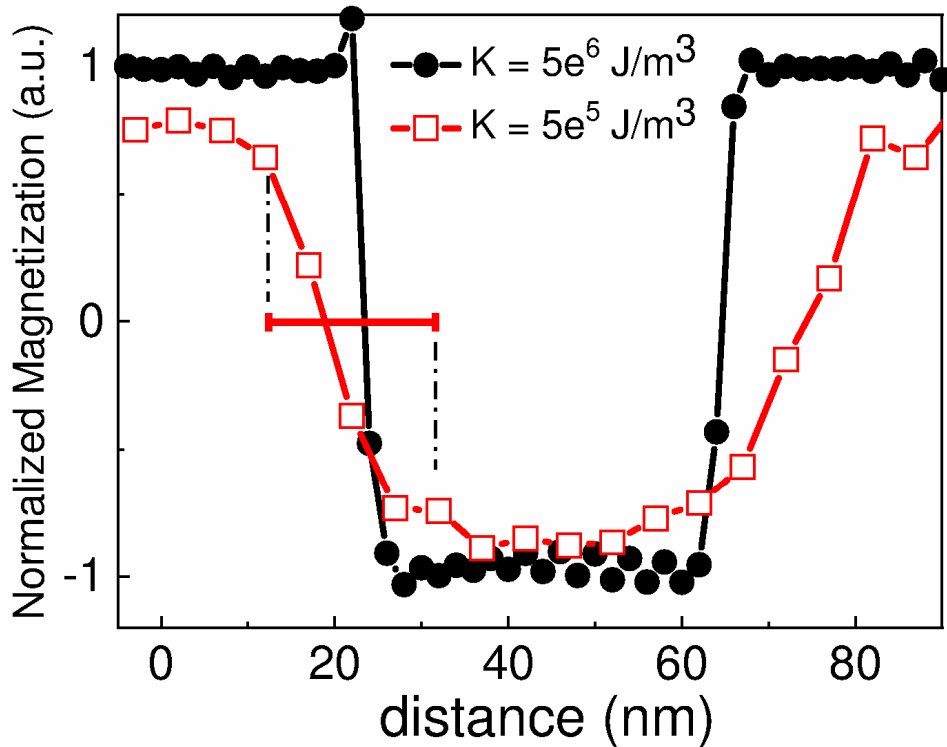


**Figure 3:** Two simulated magnetic line profiles by OOMMF micromagnetic simulations. It shows two different magnetic line profiles calculated by using realistic values of the magnetic anisotropy constants defining the system at room temperature and at an elevated temperature,  $K_m=5e6 \text{ J/m}^3$  and  $K_m=5e5 \text{ J/m}^3$ , respectively. The OOMMF simulated line profiles evidence the change of the domain wall between two up and down domains. The simulations show that at lower anisotropy (higher temperature) the domain wall thickness is broader than at high anisotropy (15 nm instead of ~3 nm).

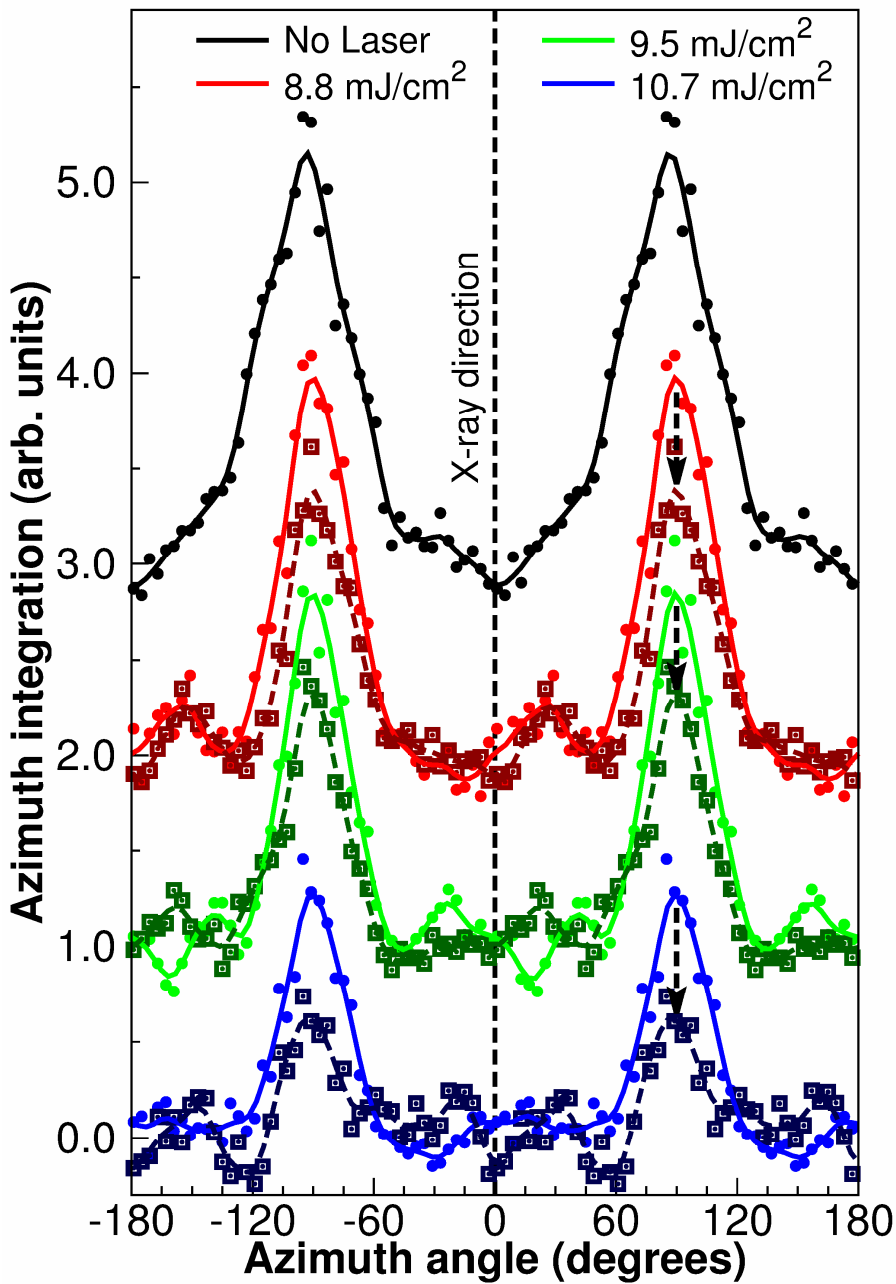


**Figure 4:** Azimuthal integration of the Fourier transform diagrams for the XMCD-PEEM images. The graphs are grouped in pairs, obtained with the same laser power (0, 8.8, 9.5, 10.7 mJ/cm<sup>2</sup>). The lines are guides to the eyes. Dots and their corresponding full lines come from the images taken at  $t = -250$  ps. Squares and dashed lines come from the images taken at  $t = +190$  ps. The dashed arrows show the intensity reduction, accounting for the reduction of the XMCD contrast in the XMCD-PEEM images.

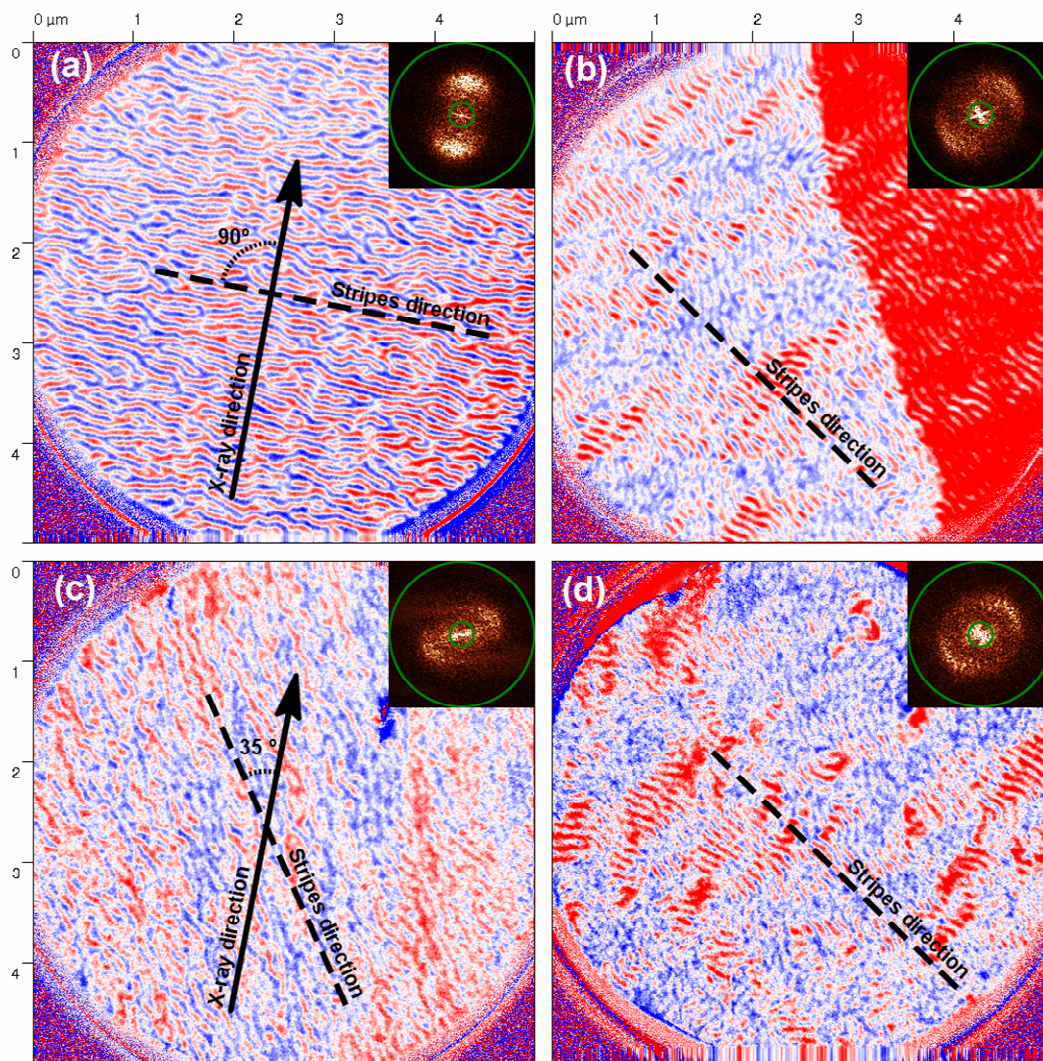


**Figure 5:**

X-PEEM images of the sample (a) with stripes oriented at  $90^\circ$  from the X-ray incidence, at room temperature (no laser applied) (b) at the same position and orientation as (a) but after pump excitation at  $18 \text{ mJ/cm}^2$ ; (c) with stripes oriented at  $35^\circ$  from the X-ray incidence, at room temperature (no laser applied) (d) at the same position and orientation as (c) but after pump excitation at  $15 \text{ mJ/cm}^2$ . The insets show the corresponding Fourier Transform of the images, which account for the preferential orientation of the stripes, and the region integrated for the azimuthal integration analysis.

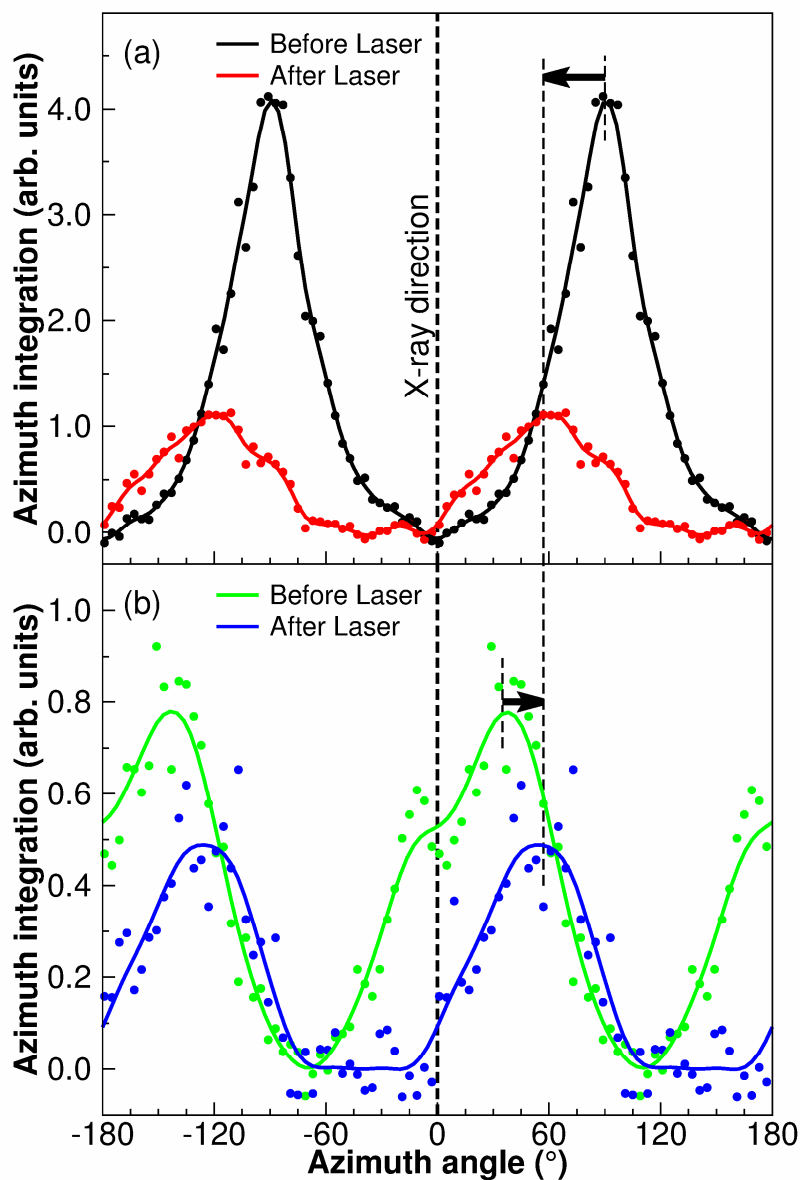


**Figure 6:** Azimuthal integration of the Fourier transform diagrams for the corresponding XMCD-PEEM images, (a) for initial orientation of the stripes of  $90^\circ$  showing in red the effect of the laser pump excitation at  $18 \text{ mJ/cm}^2$ , and (b) for initial orientation of  $35^\circ$   $90^\circ$  showing in blue the effect of the laser pump excitation at  $15 \text{ mJ/cm}^2$ . The arrows show the reorientation direction to the new stripes at  $\sim 60^\circ$ .

	XMCD @ t = -250 ps	XMCD @ t = +190 ps
No Laser	0.8 %	
8.8 mJ/cm <sup>2</sup>	9.7 %	11.3 %
9.5 mJ/cm <sup>2</sup>	5.2 %	6.7 %
10.7 mJ/cm <sup>2</sup>	3.7 %	5%

**Table 1:** mean XMCD values of the XMCD-PEEM images extracted from Figure 2

## References

- [1] E. Beaurepaire, J. C. Merle, A. Daunois, and J. Y. Bigot, *Physical Review Letters* **76**, 4250 (1996).
- [2] B. Koopmans, M. van Kampen, J. T. Kohlhepp, and W. J. M. de Jonge, *Physical Review Letters* **85**, 844 (2000).
- [3] C. Stamm, T. Kachel, N. Pontius, R. Mitzner, T. Quast, K. Holldack, S. Khan, C. Lupulescu, E. F. Aziz, M. Wiestruck *et al*, *Nature Mater.* **6**, 740 (2007)
- [4] J. Y. Bigot, M. Vomir, and E. Beaurepaire, *Nature Physics* **5**, 515 (2009).
- [5] C. D. Stanciu, F. Hansteen, A. V. Kimel, A. Kirilyuk, A. Tsukamoto, A. Itoh, and T. Rasing, *Physical Review Letters* **99** (2007).
- [6] C. Boeglin, E. Beaurepaire, V. Halte, V. Lopez-Flores, C. Stamm, N. Pontius, H. A. Dürr, and J. Y. Bigot, *Nature* **465**, 458 (2010).
- [7] V. Lopez-Flores, J. Arabski, C. Stamm, V. Halté, N. Pontius, E. Beaurepaire and C. Boeglin, *Phys. Rev. B* **86**, 014424 (2012).
- [8] T. A. Ostler, et al., *Nat. commun.* **3**,666 (2012)
- [9] S. Mangin et al. *Nature Mat.*, **13**, pages286–292(2014)
- [10] B. Vodungbo, et al., *Nature Communications* **3** (2012).
- [11] B. Vodungbo, et al., *Europhys. Lett.* **94** (2011).
- [12] N. Berggaard et al., *Phys. Rev. B* **91**, 054416 (2015)
- [13] B. Pfau, S. Schaffert, L. Muller, C. Gutt, A. Al-Shemmary, F. Buttner, R. Delaunay, S. Dusterer, S. Flewett, R. Fromter, J. Geilhufe, E. Guehrs, C. M. Gunther, R. Hawaldar, M. Hille, N. Jaouen, A. Kobs, K. Li, J. Mohanty, H. Redlin, W. F. Schlotter, D. Stickler, R. Treusch, B. Vodungbo, M. Klaui, H. P. Oepen, J. Lüning, G. Grübel, and S. Eisebitt, *Nature Communications* **3**, 1100 (2012).
- [14] J. Y. Bigot and M. Vomir, *Ann. Phys.* **525**, 2 (2013)
- [15] J. Vogel, W. Kuch, M. Bonfim, *App. Phys. Lett.* **82**, 2299 (2003)
- [16] W. Kuch, K. Fukumoto, J. Wang, F. Nolting, C. Quitmann, and T. Ramsvik, *Physical Review B* **83** (2011).
- [17] Le Guyader et al. *Journal of Electron Spectroscopy and Related Phenomena*, **185**, 371-380 (2012)

- [18] B. Wu, D. Zhu, Y. Acremann, T. A. Miller, A. M. Lindenberg, O. Hellwig, J. Stohr, and A. Scherz, *Applied Physics Letters* **99** (2011).
- [19] T. Wang, et al., *Physical Review Letters* **108** (2012).
- [20] C. von Korff. Schmising, B. Pfau, M. Schneider, C. M. Guenther, M. Giovannella, J. Perron, B. Vodungbo, L. Mueller, F. Capotondi, E. Pedersoli, N. Mahne, J. Luning, S. Eisebitt, *Phys. Rev. Lett.* **112**, 217203 (2014).
- [21] Y. Samson, A. Marty, R. Hoffmann, V. Gehanno, and B. Gilles, *Journal of Applied Physics* **85**, 4604 (1999).
- [22] V. Gehanno, R. Hoffmann, Y. Samson, A. Marty, and S. Auffret, *European Physical Journal B* **10**, 457 (1999).
- [23] H.A. Dürr, E. Dudzik, S.S. Dhesi, J.B. Goedkoop, G. van der Laan, M. Belakhovshy, C. Mocuta, A. Marty and Y. Samson, *Science* **284**, 2166 (1999).
- [24] A. Marty, Y. Samson, B. Gilles, M. Belakhovsky, E. Dudzik, E); H. Durr, S. S. Dhesi, G. van der Laan and J. B. Goedkoop, *J. Appl. Phys.* **87**, 5472 (2000).
- [25] J. R. Childress, J. L. Duvail, S. Jasmin, A. Barthelemy, A. Fert, A. Schuhl, O. Durand, and P. Galtier, *J. Appl. Phys.* **75**, 6412 (1994).
- [26] A. Hubert and R. Schäfer, *Magnetic Domains*, corr. 3rd ed. (Springer-Verlag GmbH, Heidelberg, 1998).
- [27] F. Kronast, J. Schlichting, F. Radu, S. K. Mishra, T. Noll, and H. A. Durr, *Surface and Interface Analysis* **42**, 1532 (2010).

### ***Acknowledgments:***

We are indebted for the scientific discussions with N. Bergard from IPCMS Strasbourg, concerning the OOMMF micromagnetic simulations. The authors are grateful for financial support received from the following agencies: the French CNRS-PICS program, the EU Contract Integrated Infrastructure Initiative I3 in FP6 Project No.R II 3CT-2004-50600008.